

Soldering of silicon to Invar for double-crystal monochromators

Mayara Maria Beltani Auricchio,^{a*} Paulo Roberto Mei^b and Osmar Roberto Bagnato^a

^aBrazilian Synchrotron Light Laboratory, Campinas, Sao Paulo 13083-970, Brazil, and

^bFaculty of Mechanical Engineering, University of Campinas, Campinas, Sao Paulo 13083-860, Brazil.

*Correspondence e-mail: mayara.auricchio@lnls.br

Received 13 March 2019

Accepted 6 June 2019

Edited by S. Svensson, Uppsala University, Sweden

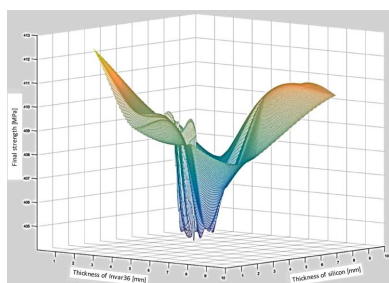
Keywords: soldering; silicon; Invar; interface; alloy.

At the Brazilian Synchrotron Light Laboratory (LNLS), new double-crystal monochromators are under development for use at the new Brazilian fourth-generation synchrotron, Sirius. The soldering technique used for the double-crystal monochromators ensures the union of monocrystalline silicon with FeNi alloy, Invar36 (64Fe–36Ni) from Grupo Metal and Invar39 (61Fe–39Fe) from Scientific Alloys, through SnSb (92.8Sn–7.2Sb), SnCu (Sn–0.3Cu) and SnBiCu (Sn–1.4Bi–0.7Cu) alloys from Nihon Superior. Following soldering tests and quantitative analysis, the Invar39/SnBiCu/Si samples were selected using base materials coated with different depositions – gold and copper. X-ray diffraction identified the formation of intermetallic compounds, such as AuSn₂ and AuSn₄ in base materials coated with gold and Cu₃Sn and Cu₆Sn₅ with copper. Before thermal cycling, the average force obtained in shear tests was 1131 N with copper deposition and 499 N with gold deposition. After five consecutive thermal cycles from room temperature down to cryogenic temperature (–196.15°C), specimens with gold deposition presented cracks in the interface region and those with copper deposition showed no defects. Based on this, qualitative and semi-quantitative analyses of specimens with copper deposition were carried out by scanning electron microscopy and energy-dispersive spectroscopy techniques to identify the composition, distribution and morphology of the elements.

1. Introduction

Double-crystal monochromators (DCMs) are composed of a pair of monocrystalline silicon crystals soldered to a base metal through a filler alloy. The base metal contains liquid-nitrogen cooling channels to dissipate the heat generated by the beam on the crystal. As monochromators work under high vacuum and at cryogenic temperatures (–196°C), the solder joint must be mechanically stable under these conditions. More information about cryogenically cooled monochromators can be found in the published literature (Bilderback *et al.*, 2000; Lee *et al.*, 2001; Zhang *et al.*, 2003; Chumakov *et al.*, 2004).

At the current Brazilian second-generation synchrotron, fixation of the monocrystalline silicon onto a copper metal base is through a gallium–indium (75.5Ga–24.5In) filler alloy. Here we propose the substitution of copper/GaIn/silicon by Invar/tin-alloy/silicon for application in monochromators. GaIn alloy is heavy, toxic and has a melting temperature of 15.7°C, below the baking temperature of the Sirius monochromator (150°C). Tin alloys have a *liquidus* temperature above the baking temperature and work at cryogenic temperatures.



© 2019 International Union of Crystallography

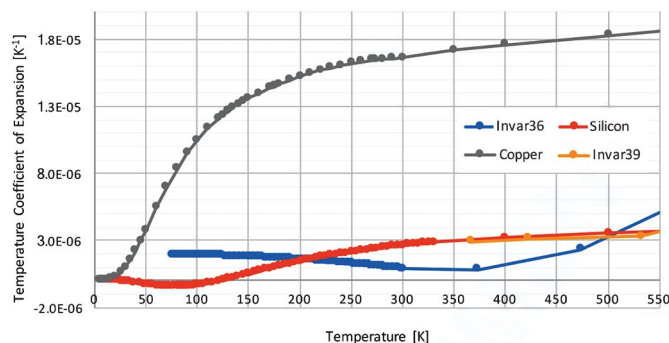


Figure 1
Temperature coefficient of expansion of the silicon, copper, Invar36 and Invar39 (data sheets of National Institute of Standards and Technology and Thomas Jefferson National Accelerator Facility).

The main difficulty in the soldering process of silicon with metals or alloys is the low coefficient of thermal expansion (CTE) of silicon. The process can generate unacceptable levels of mechanical stress that can lead to fracturing of the silicon. With this in mind, the main reason for replacing copper with Invar relates to the CTE of the materials: Invar36 (1.2×10^{-6} per $^{\circ}\text{C}$) and Invar39 (1.6×10^{-6} per $^{\circ}\text{C}$) are closer to silicon (2.3×10^{-6} per $^{\circ}\text{C}$) than copper (17.7×10^{-6} per $^{\circ}\text{C}$). Fig. 1 shows the CTE [K^{-1}] versus temperature [K] of these materials. As Invar has nearly temperature-invariant dimensions, it has been studied scientifically and used technologically (McCain & Maringer, 1965; Rosenberg, 1968; Hausch & Warlimont, 1973; Schlosser, 1971; Hausch, 1973). Invar’s unusually low thermal expansivity is related to its magnetic properties (Hausch & Warlimont, 1973). The usual thermal expansion is cancelled by magnetostriction, the coupling between magnetization and strain (Ledbetter *et al.*, 1977).

The monochromator must be operated at a constant temperature to eliminate thermal expansion, which will change the monochromated X-ray wavelength λ via Bragg’s law (Anapolsky, 2012),

$$2d \sin \theta = n\lambda. \quad (1)$$

In this equation, d refers to the spacing of lattice planes in the silicon crystal which depends on the temperature. For some materials, including silicon, there is a point at which the CTE is zero (~ 120 K for Si). This gives the intrinsic advantage of the silicon crystal having stable lattice spacing, and thus a stable monochromatic condition, over a range of a few Kelvin, which can be readily achieved by current cryogenic systems (Anapolsky, 2012).

Some authors have suggested different base materials and filler alloys for obtaining the best parameters for fixation of silicon in metallic substrates through high vacuum. Campen (2001) performed soldering tests of an Invar39/95Sn–5Sb/silicon sample using Invar39 and silicon coated with gold, while Campen (2011) reported soldering tests with an Invar36/52In–48Sn/silicon sample using base materials coated with gold. Connolley *et al.* (2009) performed tests using the following samples: copper/Al/silicon (liquid phase bonding), aluminium nitride/Al/silicon (liquid phase bonding), alumi-

nium nitride/Al/silicon (solid phase bonding), aluminium nitride/Au/silicon (eutectic brazing) and aluminium nitride/InAg/silicon (vacuum soldering). Anapolsky (2012) performed the same test as that reported by Campen (2011) on an Invar36/52In–48Sn/silicon sample, but using films of different thicknesses.

2. Materials and methods

Soldering tests of silicon plates were performed with base metals through filler alloys. Each sample was composed of base-metal/filler-alloy/silicon. The base metals used were Invar36 (ASTM F 1684-06) and Invar39 (ASTM B 753T-39). The filler alloys used were SnSb (92.8Sn–7.2Sb), SnCu (Sn–0.3Cu) and SnBiCu (Sn–1.4Bi–0.7Cu). SnCu and SnBiCu are commercially sold as Sn100C and Sn100CV, respectively.

The dimensions and geometries of the materials used in this project were reduced in relation to the monochromator prototype. The thicknesses of the Invar and silicon plate were determined from the strength generated in the Invar36/SnSb/silicon sample using the finite-element method (FEM).

According to *Metals Handbook* (ASM, 1983), the spacing between base metals is 0.03 to 0.08 mm. Based on this, the SnSb alloy with a thickness of 0.05 mm covered the whole surface of the base materials. The Invar36 and silicon plates had an area of 20 mm \times 20 mm and a thickness ranging from 0.25 to 10 mm.

Based on ASTM B 753-07 and ASTM F 1684-06 standards (ASTM, 2001, 2011), annealing for the relief of tensions of Invar36 and Invar39 was performed in a high-vacuum furnace with a heating rate of $4^{\circ}\text{C min}^{-1}$ up to 871°C (Invar39) or 899°C (Invar36) with a soak time of 15 min and cooling rate of $2^{\circ}\text{C min}^{-1}$ (Invar39) or $4^{\circ}\text{C min}^{-1}$ (Invar36).

After that, base and filler metals were cleaned with IC115 detergent in ultrasound for 15 min, washed in distilled water and dried with N_2 . Silicon was cleaned with Hexan detergent and Piranha etch, conventional composition H_2SO_4 (98%): H_2O_2 (30%), and dried with N_2 .

The base metals and silicon had coatings deposited on them to ensure that soldering was possible. According to Campen (2001), the first set of samples were obtained with base materials deposited with gold. Silicon was coated with 150 Å of Ti, 1275 Å of Ni and 3000 Å of Au, in that order, by sputtering without breaking vacuum. Invar39 was coated with 1.5 μm of Ni by electrolytic bath and 3000 Å of Au by sputtering. In the same way, based on the works of Campen (2001) and Liu *et al.* (2000), another set of samples were obtained with base materials coated with copper. Silicon was coated with 150 Å of Ti and 1275 Å of Ni by sputtering and 3000 Å of Cu by electrolytic bath. Invar39 was coated with 1.5 μm of Ni and 3000 Å of Cu by electrolytic bath.

After assembling the sample in a high-vacuum furnace at 5×10^{-6} mbar, it was heated at a rate of $1^{\circ}\text{C min}^{-1}$ up to 255°C per 15 min to ensure that the filler alloy was in the liquid state and inertial cooling. Some soldering tests were performed by pressurizing (200 kPa) during the process.

Following the soldering tests, microstructural characterization of the interface was performed to select a sample with lower porosity using an optical microscope (AxioCam MRc, Zeiss). The porosity was calculated using the Zeiss software *Axio Observer*. In order to identify the formation of the intermetallic, X-ray diffraction was carried out by Malvern Panalytical. Then, samples were submitted for shear testing to evaluate the resistance of the soldered joints with a load application speed of 0.1 mm min^{-1} in the universal testing machine EMIC DL-2000. Five consecutive thermal cycles from room temperature down to cryogenic temperatures were performed to simulate real conditions of monochromator operation. Qualitative and semi-quantitative analysis of these samples was carried out using a Quanta 650FEG scanning electron microscope using the energy-dispersive spectroscopy (EDS) technique to identify the composition, distribution and morphology of the elements.

3. Results and discussion

3.1. Geometry of materials

Fig. 2 shows the simulation results for the Invar36/SnSb/silicon sample from soldering temperature (255°C) down to cryogenic temperature (-196°C). The thicknesses of the base materials are close for stresses of 404–405 MPa for Invar36 thicknesses in the range 3.5–6 mm and silicon thicknesses of 3.5–5.5 mm. For values lower and higher than these thickness bands, there is an increase in the stress generated in the materials. Based on the minimum point of this graph, the lower stress (404.7 MPa) in the base materials was for Invar36 of thickness 5 mm and silicon of thickness 4 mm.

3.2. Soldering test and microstructural analysis

The number of samples obtained after soldering tests, the coatings of the base materials, parameters for the operation of the high-vacuum furnace and porosity of the interface region

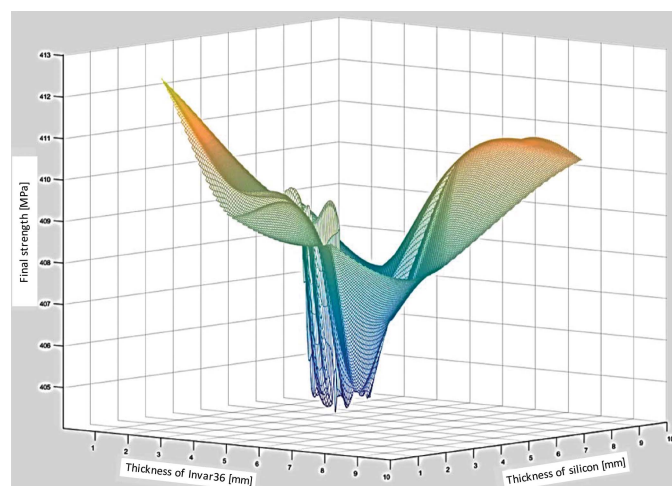


Figure 2
Graphical representation of the simulation from -196 to 255°C .

Table 1
Results of soldering tests.

Sample	Quantity	Base materials coating	Pressure (kPa)	Porosity (%)
Invar36/SnSb/silicon	1	–	0	–
Invar36/SnCu/silicon	1	–	0	–
Invar36/SnBiCu/silicon	1	–	0	–
Invar36/SnSb/silicon	4	Gold	0	31 ± 11
Invar39/SnSb/silicon	4	Gold	0	31 ± 7
Invar36/SnCu/silicon	4	Gold	0	35 ± 7
Invar39/SnCu/silicon	4	Gold	0	39 ± 5
Invar36/SnBiCu/silicon	4	Gold	0	24 ± 11
Invar39/SnBiCu/silicon	4	Gold	0	19 ± 8
Invar39/SnBiCu/silicon	5	Gold	200	4 ± 2
Invar39/SnBiCu/silicon	5	Copper	200	6 ± 3

are summarized in Table 1. For the soldering carried out without deposition of thin films in the base materials, *i.e.* for silicon and Invar36, all specimens did not present effective joints. In the soldering carried out with deposition of gold in silicon and Invar36 or Invar39 and without pressurizing, all specimens had effective junctions. The Invar39/SnBiCu/silicon specimen had the lowest porosity in the interface region (19%). The repetition of the soldering test with the Invar39/SnBiCu/silicon specimen and under 200 kPa pressure was effective and the porosity in the interface region reduced from 19% to 4%. The soldering test of the Invar39/SnBiCu/silicon specimen with copper deposition in the base materials and under a pressure of 200 kPa was also effective and presented a porosity in the interface region of 6%. Based on the porosity of the interface region, the Invar39/SnBiCu/silicon samples under 200 kPa pressure using base materials coated with gold and copper were selected for further testing. Porosity is a relevant factor for the operation of the monochromator because it can generate the accumulation of gases and decrease the thermal transfer between the silicon and Invar.

In the soldering carried out without deposition of thin films in the base materials, tin alloys (SnSb, SnCu and SnBiCu) adhered to the Invar36 but they did not adhere to the silicon. Based on this, the interface between silicon and tin was analyzed. Curves of the solid solubility of some chemical elements in the silicon, presenting low solubility in solid silicon even at high temperatures, have been given by Trumbore (1960). The solubility of the tin in the silicon at 600°C is of the order of $10^{19} \text{ atoms cm}^{-3}$. From this, and the properties of both elements, the atomic percent of tin in silicon is 0.02% and the mass percent is 0.08%. These calculated values are in accordance with the values of the silicon–tin phase diagram of Fig. 3, where it is also observed that there is practically no solubility in all composition bands of the silicon in the tin.

The low solubility of tin in silicon is due to the size of the atoms and their crystalline structures. In relation to the atomic radius of these chemical elements (0.1153 nm for silicon and 0.16200 nm for tin), the tin atom is 40% larger than the silicon atom. The crystalline structure of the silicon is face-centered cubic whereas the tin has different allotropic forms. Below 13.2°C , Sn- α has a cubic crystalline face-centered structure.

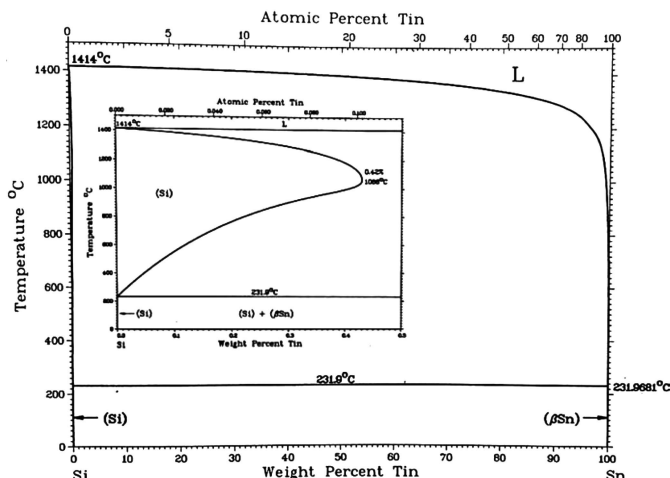


Figure 3 Phase diagram of the Si–Sn system (Olesinski & Abbaschian, 1984). Reprinted by permission from Springer Nature.

Between 13.2 and 161°C, Sn-β is body-centered tetragonal. Above 161°C, Sn-γ has a rhombic structure. Therefore, silicon and tin have different crystalline structures at soldering temperature (255°C).

The diffusivity of tin, bismuth and antimony in the silicon at 1000°C is also very low, of the order of 10^{-15} to 10^{-16} $\text{cm}^2 \text{s}^{-1}$, as shown in Fig. 4. On the other hand, the diffusivity of copper in silicon is 10^{-6} $\text{cm}^2 \text{s}^{-1}$ at 1000°C. However, copper is the minor component in these alloys, with content of less than 0.7% weight percent. The diffusivity D of the tin in silicon at 1000°C can also be calculated by the following Yeh equation,

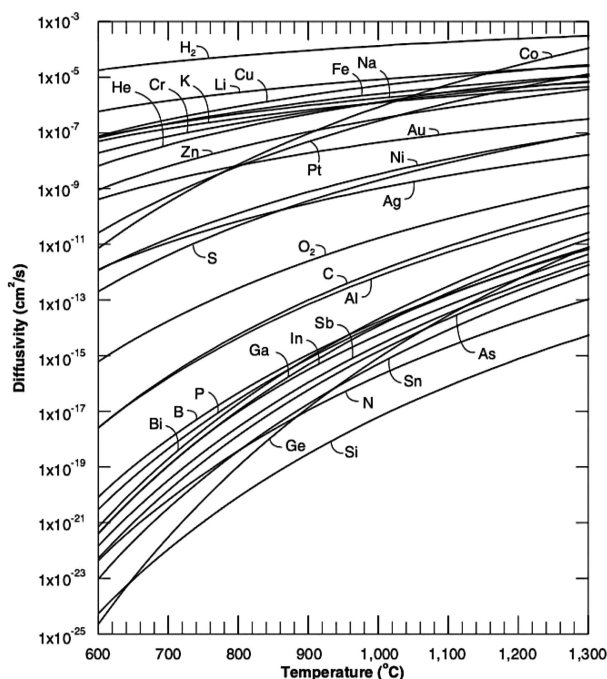


Figure 4 Diffusivities of selected impurities in silicon versus temperature (Jones, 2008). Reprinted by permission from IC Knowledge LLC.

being in agreement with the data calculated by Akasaka *et al.* (1974),

$$\begin{aligned}
 D &= 32 \exp(-98000/RT) \text{ cm}^2 \text{ s}^{-1} \\
 &= 32 \exp[-98000/(1.987 \times 1273)] \\
 &= 5 \times 10^{-16} \text{ cm}^2 \text{ s}^{-1}.
 \end{aligned}
 \tag{2}$$

3.3. X-ray diffraction

X-ray diffraction identified the formation of intermetallic compounds. Fig. 5 shows diffractograms of the interface region between silicon with (a) Ti/Ni/Au-deposition/SnBiCu and (b) Ti/Ni/Cu-deposition/SnBiCu. The reaction between the film deposited and the filler resulted in the presence of intermetallic phases, such as AuSn_2 and AuSn_4 [Fig. 5(a)] and Cu_3Sn and Cu_6Sn_5 [Fig. 5(b)].

Robertson & Karnowsky (1968) investigated the gold interdiffusion with the 63%Sn–37%Pb alloy at temperatures of 121 and 195°C. All three intermetallic compounds – AuSn , AuSn_2 and AuSn_4 – were observed in the tin–gold diffusion pair. The intermetallic phase AuSn_4 was observed to have Kirkendall porosity.

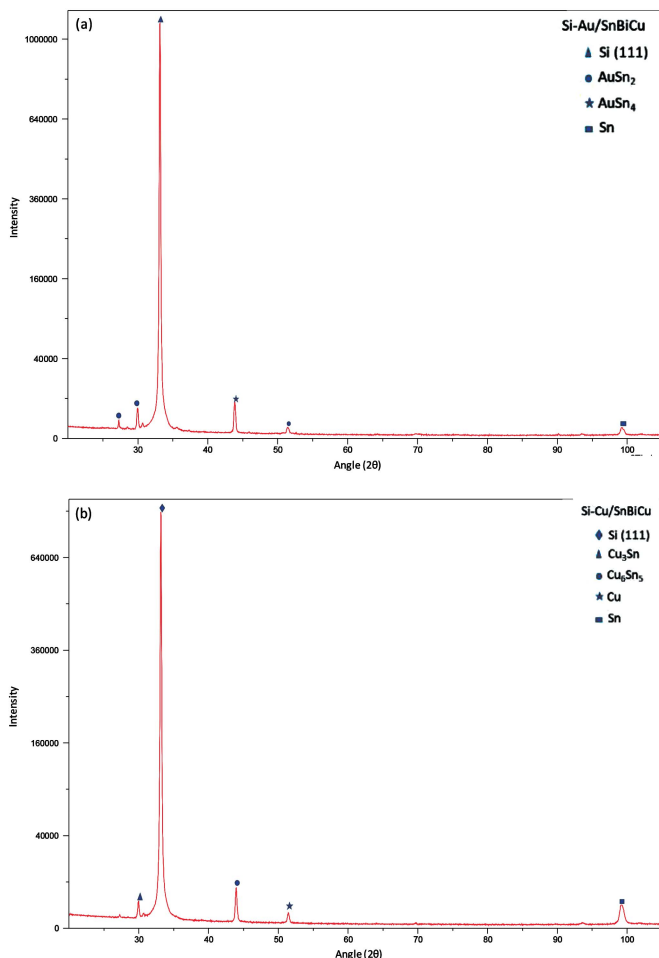


Figure 5 X-ray diffraction of the interface region between silicon with (a) Ti/Ni/Au deposition/SnBiCu and (b) Ti/Ni/Cu deposition/SnBiCu.

Table 2

Results of shear test before thermal cycling: maximum shear force (N).

Gold deposition	Copper deposition
723	1401
663	1233
468	954
141	936
Average 499 ± 114	Average 1131 ± 98

Liu *et al.* (2000) studied the wettability reaction of the SnPb eutectic alloy on the silicon surface with copper deposition. After annealing the samples at 200°C for 1 to 40 minutes, Cu₃Sn and Cu₆Sn₅ intermetallics were formed due to the reaction between the copper layer and the tin-based alloy. Cu₃Sn appeared in clusters containing voids in the center of these clusters. The appearance of voids is due to the diffusion of copper atoms during the growth of Cu₃Sn. The Cu₆Sn₅ compound grew continuously in a direction perpendicular to the silicon surface and gradually transformed into a columnar morphology by increasing the annealing time.

3.4. Shear test before thermal cycling

As shown by Auricchio *et al.* (2018), the base materials did not show any type of defect after the shear test and the rupture of the specimens occurred in the soldering region. Table 2 shows the maximum shear force obtained from each sample, Invar39/SnBiCu/silicon, using base materials with gold film and copper film. Samples with gold film deposited on base materials presented an average force of 499 N and with copper film presented an average of 1131 N. Therefore, the mechanical strength of samples with the copper film is higher than the others.

The difference between these specimens is the coating material, *i.e.* gold and copper. Therefore, this is the main factor to be analyzed for the justification of the mechanical resistance in the region of soldering between the materials involved.

According to Schwartz (2014), copper lowers the melting point, improves fatigue resistance under thermal cycling, improves wetting and reduces the rate of dissolution of copper from the parts being soldered. However, it forms intermetallics, promotes tin whiskers, makes solders sluggish and gritty, and degrades wetting. Gold dissolves easily, forms intermetallics, and lowers the melting point of tin-based solders. Alloys with higher proportions of tin can accept more gold without becoming brittle. According to Campen (2001), gold has a high affinity for tin, so it will readily dissolve on heating and promote wetting. It can form AuSn₄, which is a brittle material.

Although the filler alloy used does not contain gold in its chemical composition, there is a reaction between

the gold film of the base materials and the filler, forming the intermetallic AuSn₄. Thus, the lower strength of metalized joints with gold is probably due to the formation of the brittle intermetallic AuSn₄ in the soldering region.

3.5. Microstructural analysis after thermal cycling

After the soldering test, the thermal cycling test was performed with four samples composed of Invar39/SnBiCu/silicon, two samples with gold deposition and two with copper deposition. All samples with gold deposition presented interfacial defects, which did not occur with the other samples.

In Fig. 6, the soldering interfaces among Invar39, SnBiCu and silicon using base materials with gold deposition (left image) and copper deposition (right image) obtained by optical microscope are shown.

Invar39/SnBiCu/silicon samples using base materials coated with gold deposition (Fig. 6, left side) presented cracks in the soldering region and no defects were found in the base materials. Fragile fractures begin at the interface between the filler alloy and the silicon, propagate in the soldering region, and are adjacent to the surface of the silicon. These cracks are probably due to the formation of the brittle AuSn₄ intermetallic in the soldering region. Samples using base materials coated with copper deposition (Fig. 6, right side) showed no defects in the soldering region and a uniform interface between Invar39/SnBiCu.

Fig. 7(a) shows the soldering interfaces among silicon, SnBiCu and Invar39 using base materials with copper deposition obtained using a Quanta scanning electron microscope and the EDS technique. The intensities of elements in the filler alloy are presented. The elements identified in the quantitative analysis were silicon, nickel, iron, tin and copper. Tin [Fig. 7(e)] and copper [Fig. 7(f)] come from the filler alloy, and copper was also present in the coating of the base materials. Iron [Fig. 7(d)] and nickel [Fig. 7(c)] are elements from Invar39, and nickel was also present in the coating of the base materials. As bismuth had a low concentration, it was not possible to evaluate its distribution in the chemical mapping.

Silicon [Fig. 7(b)] hardly diffuses in the soldering region. There is diffusion of iron [Fig. 7(d)] in the soldering region, but as it moves away from Invar39 the iron content gradually

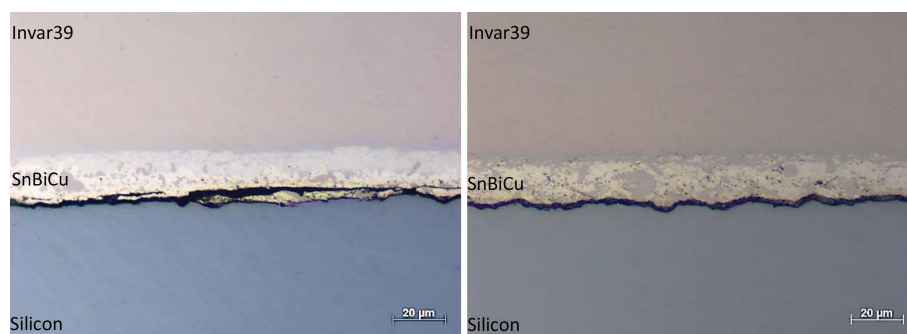


Figure 6

Micrographs of Invar39/SnBiCu/silicon samples after thermal cycling by an optical microscope. The left side shows the sample with gold film and the right side that with copper film.

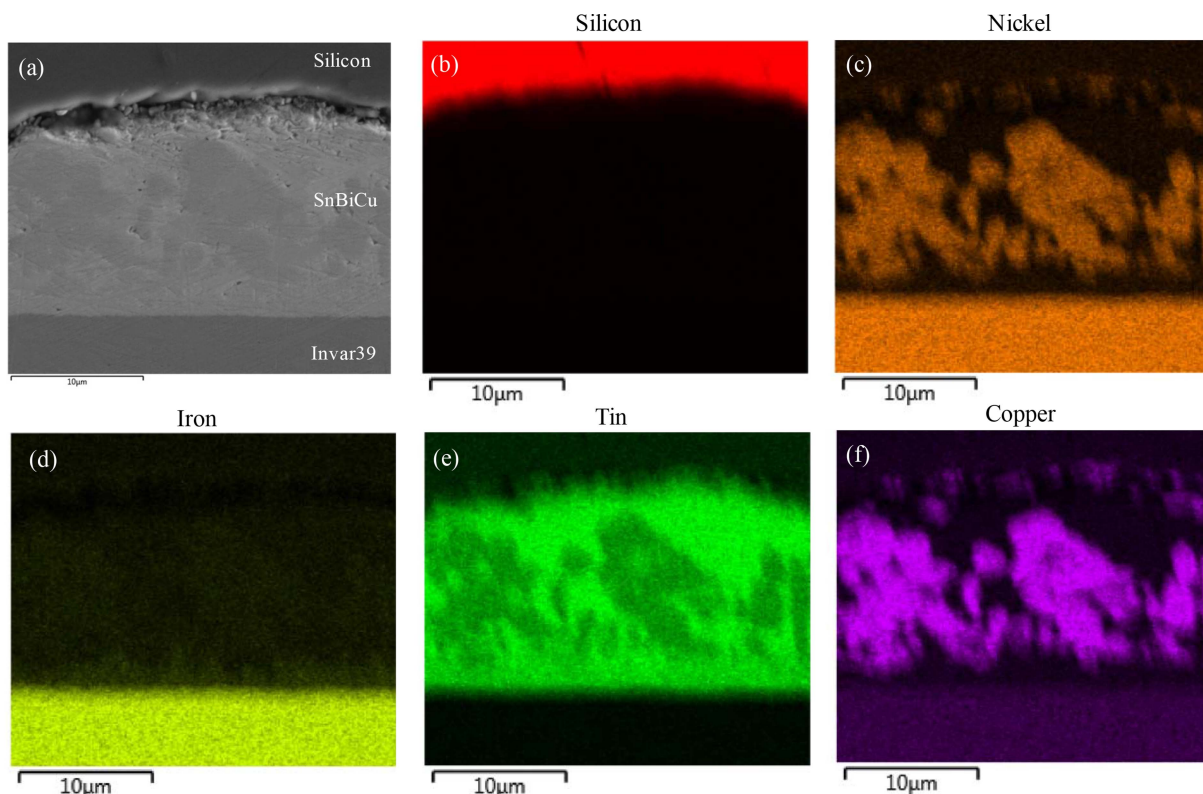


Figure 7 Chemical mapping of the soldering interface of the Invar39/SnBiCu/silicon sample after thermal cycling using a Quanta scanning electron microscope.

decreases. On the other hand, where tin [Fig. 7(e)] appears, there is a lower content of nickel [Fig. 7(c)] and copper [Fig. 7(f)]. The tin does not diffuse into iron, but it does diffuse into silicon.

Nickel [Fig. 7(c)] and copper [Fig. 7(f)] appear in the soldering region because these elements have the same crystalline structure (face-centered cubic), similar sizes (atomic radius of copper = 1.28 Å and nickel = 1.24 Å) and form a substitutional solid solution. From the copper–nickel phase diagram of Fig. 8, copper and nickel form a solid substitutional solution in all composition bands, because the copper atoms replace positions that are occupied by nickel atoms.

4. Conclusions

Silicon plates were soldered with Invar36 and Invar39 using different types of filler alloys – SnSb, SnCu and SnBiCu. The best parameters were Invar39/SnBiCu/silicon samples at pressures of 200 kPa using base materials coated with different films – gold and copper. In the X-ray diffraction experiments, intermetallic compounds were identified in the soldering interface silicon/SnBiCu, such as AuSn₂ and AuSn₄ in base materials coated with gold and Cu₃Sn and Cu₆Sn₅ for those coated with copper. In the shear test, the specimens with copper film presented higher shear strengths than the others. The average force obtained in shear tests was 1131 N with copper deposition and 499 N with gold deposition. After thermal cycling, samples using base materials with gold deposition presented cracks in the soldering region, possibly

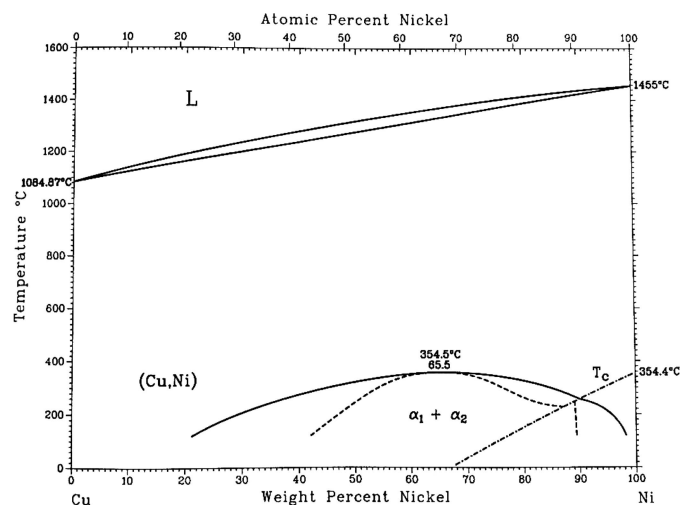


Figure 8 Binary Cu–Ni phase diagram (Chakrabarti *et al.*, 1991). Reprinted with permission from ASM International.

from the formation of brittle intermetallic AuSn₄. Microstructural analysis identified the chemical composition of the interface region of the Invar39/SnBiCu/silicon sample with base materials coated with copper using the EDS technique. Tin has greater diffusion with silicon than Invar39. Nickel and copper appear together in the soldering region because these elements form a substitutional solid solution. Furthermore, the highest concentrations of these elements in this region are replacing part of the tin. In future work, development and

precise definition of a prototype will be performed to ensure the efficiency under the best conditions of operation of the monochromator in the light line. These results showed the potential feasibility of replacing the silicon/GaIn/copper assembly with the silicon/SnBiCu/Invar39 on a reduced-scale, but real-scale testing will be necessary.

Funding information

The authors would like to thank the Coordination of Improvement of Higher Education Personnel (CAPES) (Grant No. 88882.143464/2017-01), Brazilian Center for Research in Energy and Materials (CNPEM), and University of Campinas (UNICAMP) for their financial support of this project.

References

- Akasaka, Y., Horie, K., Nakamura, G., Tsukamoto, K. & Yukimoto, Y. (1974). *Jpn. J. Appl. Phys.* **13**, 1533–1540.
- Anapolsky, A. S. (2012). *Bonding of Silicon to Invar36 for LN Cryogenic Monochromators*, pp. 1–2. Stanford Linear Accelerator Center, Menlo Park, CA, USA.
- ASM (1983). *Metals Handbook: Welding, Brazing and Soldering*, 9th ed., pp. 927–976. Materials Park, Ohio: American Society for Metals.
- ASTM (2001). *Standard Specification for Thermostat Component Alloys*, p. 4. ASTM B 753–07. ASTM International, West Conshohocken, PA, USA.
- ASTM (2011). *Standard Specification for Iron-Nickel and Iron-Nickel-Cobalt Alloys for Low Thermal Expansion Applications*, p. 8. ASTM F 1684–06. ASTM International, West Conshohocken, PA, USA.
- Auricchio, M. M. B., Bagnato, O. R. & Mei, P. R. (2018). *Defect Diffusion Forum*, **389**, 176.
- Bilderback, D. H., Freund, A. K., Knapp, G. S. & Mills, D. M. (2000). *J. Synchrotron Rad.* **7**, 53–60.
- Campen, D. G. V. (2001). *Low Stress Soldering Invar to Silicon*, pp. 1–16. Stanford Synchrotron Radiation Laboratory, Menlo Park, CA, USA.
- Campen, D. G. V. (2011). *Bonding Silicon to Invar for LN Cryogenic Manifold*, pp. 1–12. Stanford Synchrotron Radiation Laboratory, Menlo Park, CA, USA.
- Chakrabarti, D. J., Laughlin, D. E., Chen, S. W. & Chang, Y. A. (1991). *Phase Diagrams of Binary Nickel Alloys*, pp. 85–95. Materials Park: ASM International.
- Chumakov, A., Rüffer, R., Leupold, O., Celse, J.-P., Martel, K., Rossat, M. & Lee, W.-K. (2004). *J. Synchrotron Rad.* **11**, 132–141.
- Connolley, T., Hanks, S., Drakopoulos, M. & Hill, T. (2009). *Sci. Technol. Weld. Joining*, **14**, 1–3.
- Hausch, G. (1973). *Phys. Status Solidi A*, **15**, 501–510.
- Hausch, G. & Warlimont, H. (1973). *Z. Metallkd.* **64**, 152.
- Jones, S. W. (2008). *Diffusion in Silicon*, p. 57. IC Knowledge LLC, Georgetown, MA, USA.
- Ledbetter, H. M., Naimon, E. R. & Weston, W. F. (1977). *Adv. Cryog. Eng.* **22**, 174.
- Lee, W.-K., Fezzaa, K., Fernandez, P., Tajiri, G. & Mills, D. M. (2001). *J. Synchrotron Rad.* **8**, 22–25.
- Liu, C. Y., Tu, K. N., Sheng, T. T., Tung, C. H., Frear, D. R. & Elenius, P. (2000). *J. Appl. Phys.* **87**, 750–754.
- McCain, W. S. & Maringer, R. E. (1965). *Mechanical and Physical Properties of Invar and Invar Type Alloys*. DMIC Memorandum 207. Defense Metals Information Center, Columbus, OH, USA.
- Olesinski, R. W. & Abbaschian, G. J. (1984). *Bull. Alloy Phase Diagrams*, **5**, 273–276.
- Robertson, M. M. & Karnowsky, M. M. (1968). *Gold-Tin and Gold-Tin-Lead Diffusion Couples*, p. 38. SC-TM-68-728. Sandia National Laboratories, Albuquerque, NM, USA.
- Rosenberg, S. J. (1968). *Nickel and Its Alloys*. NBS Monograph 106, USGPO. Gaithersburg: National Bureau of Standards.
- Schlosser, W. F. (1971). *J. Phys. Chem. Solids*, **32**, 939–949.
- Schwartz, M. M. (2014). *Soldering – Understanding the Basics*, pp. 1–29. Materials Park: ASM International.
- Trumbore, F. A. (1960). *Bell Syst. Tech. J.* **39**, 205–233.
- Zhang, L., Lee, W.-K., Wulff, M. & Eybert, L. (2003). *J. Synchrotron Rad.* **10**, 313–319.